Sensorless speed control of permanent-magnet motors with nonsinusoidal EMF waveform

C.H. De Angelo, G.R. Bossio, J.A. Solsona, G.O. García and M.I. Valla

Abstract: A novel sensorless speed-control strategy for permanent-magnet AC motors (PMACMs) is presented. A nonlinear reduced-order observer and a high-gain observer are designed to estimate the induced EMF, without mechanical position or speed sensors. In contrast with previous proposals, the EMF estimation is performed without previous knowledge of its waveform. From the estimated EMF, the rotor speed and the position derivatives of flux are calculated and used for the implementation of a PMACM speed control without mechanical position sensor. The proposed strategy is not limited to PMACM with sinusoidal or trapezoidal EMF waveform. Moreover, it allows the PMACM ripple torque and copper losses to be minimised. The performance of the proposal is validated through simulation and experimental results.

1 Introduction

Permanent-magnet AC-motor (PMACM) drives are widely used in high-performance applications. These motors are preferred because of the absence of rotor windings, their high efficiency, their high torque-to-inertia ratio and their power density.

However, an important disadvantage of PMACMs is their torque pulsations. This pulsating torque is produced by different reasons [1, 2]:

(*a*) distortion of the actual airgap-flux waveform with regard to the ideal waveform due to the motor geometry;

(*b*) distortion of the excitation currents due to the invertor commutation and the current controller;

(*c*) low resolution or offset in the current measurement;

(*d*) delay in the synchronisation between the excitation currents and the actual rotor position; and

(*e*) magnetic reluctance variation due to stator slots and other irregularities.

The pulsating torque produced by the interaction of stator-current magnetomotive forces and rotor-magnet flux distribution or the angular variation in the rotor magnet reluctance is called 'ripple torque'. The pulsating torque generated by the interaction of the rotor magnetic flux and angular variations in the stator magnetic reluctance is known as 'cogging torque' [1]. Recently, different techniques have been proposed to reduce torque pulsations. These techniques can be divided into two groups [1–3]:

(i) motor-design techniques; and

(ii) active control techniques.

Motor-design techniques allow an important reduction of cogging torque, though its complete elimination is not possible. Within the second group, several techniques, such as preprogrammed stator-current excitations to cancel the torque harmonic components [4–6], torque estimation based on model reference adaptive schemes [7] and iterative learning control [3], have been proposed.

In [8], a programmed current-waveform control strategy for ripple torque and 'copper-loss' minimisation is proposed. In this proposal, excitation currents, synchronised with rotor position, are calculated on the basis of the instantaneous-reactive-power theory [9]. The implementation of this strategy requires a previous knowledge of the position derivative of the linked-flux waveform (induced electromotive force divided by speed), and the use of a position sensor to generate the excitation-current references. The use of a position sensor increases the drive costs and reduces its mechanical robustness. This is the main reason why several PMACM control techniques are used which avoid the use of mechanical position or speed sensors. These proposals are applicable to PMACMs whose induced electromotive force (EMF) is perfectly sinusoidal or trapezoidal [10], but they do not take into consideration the case of PMACMs with other EMF waveforms.

In this work, a novel sensorless speed-control strategy for PMACM is presented. A nonlinear reduced-order observer and a high-gain observer are designed to estimate the induced EMF, without mechanical position or speed sensors. From the estimated EMF, the rotor speed and the position derivatives of flux are calculated, and used in the implementation of a PMACM speed control without mechanical position sensor. The main advantage of the strategy proposed in this paper is that the controller does not need information about the motor-EMF waveform, as is usually required when an observer for high performance

© IEE, 2005

IEE Proceedings online no. 20050023

doi:10.1049/ip-epa:20050023

Paper first received 25th January and in final revised form 26th April 2005

C.H. De Angelo, G.R. Bossio and G.O. García are with CONICET and also with Grupo de Electrónica Aplicada GEA, Facultad de Ingeniería, UNRC, Ruta Nacional #36 Km. 601, X5804BYA, Río Cuarto, Argentina

J.A. Solsona is with CONICET and also with Departamento de Ingeniería Eléctrica y de Computadoras, Instituto de Investigaciones en Ingeniería Eléctrica Alfredo Desages, UNS, Av. Alem 1253 (8000), Bahía Blanca, Argentina

M.I. Valla is with CONICET and also with Departamento de Electrotecnia, Laboratorio de Electrónica Industrial, Control e Instrumentación (LEICI), Facultad de Ingeniería, UNLP, 1900, La Plata, Argentina

E-mail: cdeangelo@ieee.org

is to be designed. This waveform does not necessarily need to be sinusoidal or trapezoidal, as other proposals reported in the literature do; indeed it can take any shape. As a consequence, the strategy is very robust in the face of the uncertainty in the EMF waveform. This waveform does not always coincide with that reported by the manufacturer; it is even possible to replace a motor having a different EMF waveform, without performing a laboratory or a self-commissioning test to know the new EMF waveform. In addition, this proposal does not need to use a mechanical position or speed sensor, allowing PMACM ripple-torque and copper-loss minimisation.

2 Permanent-magnet AC-motor model and control strategy

2.1 Model

In order to develop the control strategy, the dynamic model of a PMACM is written in a stationary reference frame α–β–0 [11]:

$$\left.\begin{aligned} \frac{di_\alpha}{dt} &= -\frac{R}{L}i_\alpha - \frac{1}{L}e_\alpha + \frac{1}{L}v_\alpha \\ \frac{di_\beta}{dt} &= -\frac{R}{L}i_\beta - \frac{1}{L}e_\beta + \frac{1}{L}v_\beta \\ 0 &= -e_0 + v_0 \end{aligned}\right\} \tag{1}$$

$$\left.\begin{aligned} \frac{d\theta}{dt} &= \omega \\ \frac{d\omega}{dt} &= \frac{1}{J}T_e - \frac{B}{J}\omega - \frac{1}{J}T_L \end{aligned}\right\} \tag{2}$$

where, i_α, i_β, e_α, e_β, e_0, v_α, v_β, v_0 represent the current, EMF and voltage components, respectively, in the stationary reference frame α–β–0; R and L are the stator resistance and inductance, respectively; θ, ω and T_e represent the rotor position and speed, and the electromagnetic torque produced by the motor; J and B are inertia and viscosity, respectively; and T_L is the load torque.

Despite the fact that the motor has no connection to the neutral point, and therefore no zero-current component can exist, the equation corresponding to the zero-voltage component is included in the motor model (1). This permits the extraction of some additional information about the harmonic components that exist in the phase-to-neutral EMF waveform.

The EMF induced into the stator windings can be obtained as the time derivative of the linked flux:

$$\left.\begin{aligned} e_\alpha &= \frac{\partial\lambda_\alpha}{\partial\theta}\frac{d\theta}{dt} = \phi_\alpha(\theta)\omega \\ e_\beta &= \frac{\partial\lambda_\beta}{\partial\theta}\frac{d\theta}{dt} = \phi_\beta(\theta)\omega \\ e_0 &= \frac{\partial\lambda_0}{\partial\theta}\frac{d\theta}{dt} = \phi_0(\theta)\omega \end{aligned}\right\} \tag{3}$$

where, λ_α, λ_β and λ_0 are the linked-flux components. The position derivatives of the linked flux, $\phi_i(\theta)(i = \alpha, \beta, 0)$, are functions of the rotor position and depend on the motor construction.

The electromagnetic torque can be expressed by [11]

$$T_e = \phi_\alpha(\theta)i_\alpha + \phi_\beta(\theta)i_\beta \tag{4}$$

Therefore it is evident that, to obtain a constant torque, currents whose waveform depends on the functions ϕ_α and ϕ_β must be imposed.

2.2 Minimum-ripple-torque-control strategy

The ripple-torque-minimisation strategy presented in this work is based on that proposed in [8]. The motor control is carried on by imposing stator currents whose waveforms, synchronised with the rotor position, are calculated on the basis of the instantaneous-reactive-power theory [9]. Considering that the torque developed by the motor depends on the instantaneous active power, the motor torque is controlled by manipulating the active-current components. On the other hand, instantaneous reactive power does not contribute to torque development, but produces reactive-current circulation. Therefore, instantaneous-reactive-current components are set to zero to minimise copper losses.

For the implementation of this strategy, stator-current references are calculated by the expressions

$$\left.\begin{aligned} i_\alpha^* &= \frac{T_e^*\phi_\alpha}{\phi_\alpha^2 + \phi_\beta^2} \\ i_\beta^* &= \frac{T_e^*\phi_\beta}{\phi_\alpha^2 + \phi_\beta^2} \end{aligned}\right\} \tag{5}$$

where variables x^* represent the reference of x. A more detailed development of this expression can be found in [8].

To implement this control scheme, it is necessary to know the position derivatives of the linked flux $\phi_i(\theta)(i = \alpha, \beta, 0)$. Using a position sensor, $\phi_i(\theta)$ can be determined 'offline' in an experimental way for each particular motor, and stored in a look-up table to permit easy calculation of the current references according to (5). However, the goal of the present proposal is to design a control law that avoids the use of linked flux and rotor-position sensors. For this reason, an observer is used for obtaining estimates for those variables. These estimates replace the position derivatives of linked flux and speed values in the control law.

3 Proposed observer

To avoid the use of linked flux and mechanical-position sensors, it is necessary to estimate the rotor speed and the position derivatives of flux from the electrical measurable variables. The rotor speed is needed to close the speed-control loop, and position derivatives of flux are needed to generate the current references to minimise the ripple torque and copper losses (5).

As it can be seen in (3), the information about rotor speed and position derivatives of flux (ϕ functions) can be obtained from the induced EMF [12]. To do that, a novel nonlinear observer is proposed in this paper. This proposal uses a nonlinear reduced-order observer and a high-gain observer to estimate the induced EMF without previous knowledge of its waveform, measuring motor currents and voltages. Once the EMF is estimated, the position derivatives of the linked flux and the rotor speed are calculated.

The time derivatives of the induced EMF components α–β in (3) are first calculated to implement the observer:

$$\left.\begin{aligned} \frac{de_\alpha}{dt} &= \frac{d\phi_\alpha}{dt}\omega + \phi_\alpha\frac{d\omega}{dt} \\ \frac{de_\beta}{dt} &= \frac{d\phi_\beta}{dt}\omega + \phi_\beta\frac{d\omega}{dt} \end{aligned}\right\} \tag{6}$$

From (6), the following EMF observer can be designed:

$$\left.\begin{aligned}\frac{d\hat{e}_\alpha}{dt} &= \frac{d\hat{\phi}_\alpha}{dt}\hat{\omega} + \hat{\phi}_\alpha\frac{d\hat{\omega}}{dt} + g\left(L\frac{d\hat{i}_\alpha}{dt} - L\frac{di_\alpha}{dt}\right)\\ \frac{d\hat{e}_\beta} {dt} &= \frac{d\hat{\phi}_\beta}{dt}\hat{\omega} + \hat{\phi}_\beta\frac{d\hat{\omega}}{dt} + g\left(L\frac{d\hat{i}_\beta}{dt} - L\frac{di_\beta}{dt}\right)\end{aligned}\right\} \quad (7)$$

where $(\wedge)$ stands for estimated variables and g is a constant value. The observer copies the EMF dynamics, and employs the error between estimated and actual current derivatives as a correction term. Note that e_0 is not estimated, since it can be calculated on the basis of voltage measurements.

The time derivatives of the estimated currents, used in the correction term of the observer, can be calculated from (1):

$$\left.\begin{aligned}\frac{d\hat{i}_\alpha}{dt} &= -\frac{R}{L}i_\alpha - \frac{1}{L}\hat{e}_\alpha + \frac{1}{L}v_\alpha\\ \frac{d\hat{i}_\beta}{dt} &= -\frac{R}{L}i_\beta - \frac{1}{L}\hat{e}_\beta + \frac{1}{L}v_\beta\end{aligned}\right\} \quad (8)$$

The time derivative of the estimated speed (acceleration, $\hat{a}$) can be obtained from (2) and (4), assuming that no load torque exists ($T_L = 0$):

$$\hat{a} = \frac{d\hat{\omega}}{dt} = \frac{1}{J}\left(\hat{\phi}_\alpha i_\alpha + \hat{\phi}_\beta i_\beta\right) - \frac{B}{J}\hat{\omega} \quad (9)$$

The calculus of the time derivative of the measured currents, used in the correction term (7), could introduce estimation errors, due to the measured current ripple and measurement noise. To reduce this error, the following change of variable is proposed:

$$\left.\begin{aligned}\hat{\xi}_\alpha &= \hat{e}_\alpha + gLi_\alpha\\ \hat{\xi}_\beta &= \hat{e}_\beta + gLi_\beta\end{aligned}\right\} \quad (10)$$

where $\hat{\xi}_\alpha$, $\hat{\xi}_\beta$ are auxiliary variables.

Differentiating (10), and substituting the derivatives defined in (7) and (8), the proposed observer results in

$$\left.\begin{aligned}\frac{d\hat{\xi}_\alpha}{dt} &= \frac{d\hat{\phi}_\alpha}{dt}\hat{\omega} + \hat{\phi}_\alpha\hat{a} + g(-Ri_\alpha - \hat{e}_\alpha + v_\alpha)\\ \frac{d\hat{\xi}_\beta}{dt} &= \frac{d\hat{\phi}_\beta}{dt}\hat{\omega} + \hat{\phi}_\beta\hat{a} + g\left(-Ri_\beta - \hat{e}_\beta + v_\beta\right)\end{aligned}\right\} \quad (11)$$

To obtain the time derivatives of $\hat{\phi}$, a reduced-order high-gain observer is proposed, which is essentially an approximate 'differentiator' [13]. It is designed by employing the variable $\tilde{\phi}$ as an estimate of $\hat{\phi}$, and using its derivative $(d\tilde{\phi}/dt)$ as the estimate of $(d\hat{\phi}/dt)$. The reader can refer to Appendix 1 (Section 9.1) for a detailed development of the following expressions:

$$\left.\begin{aligned}\frac{d\hat{\chi}_\alpha}{dt} &= -\frac{1}{\varepsilon}\left(\hat{\chi}_\alpha + \frac{1}{\varepsilon}\hat{\phi}_\alpha\right)\\ \frac{d\hat{\chi}_\beta}{dt} &= -\frac{1}{\varepsilon}\left(\hat{\chi}_\beta + \frac{1}{\varepsilon}\hat{\phi}_\beta\right)\end{aligned}\right\} \quad (12)$$

where $\hat{X}_\alpha$, $\hat{X}_\beta$ are auxiliary variables, and ε is a small positive parameter. Then,

$$\left.\begin{aligned}\frac{d\hat{\phi}_\alpha}{dt} &\approx \frac{d\tilde{\phi}_\alpha}{dt} = \hat{\chi}_\alpha + \frac{1}{\varepsilon}\hat{\phi}_\alpha\\ \frac{d\hat{\phi}_\beta}{dt} &\approx \frac{d\tilde{\phi}_\beta}{dt} = \hat{\chi}_\beta + \frac{1}{\varepsilon}\hat{\phi}_\beta\end{aligned}\right\} \quad (13)$$

Thus, the EMF observer will be given by

$$\left.\begin{aligned}\frac{d\hat{\xi}_\alpha}{dt} &= \left(\hat{\chi}_\alpha + \frac{1}{\varepsilon}\hat{\phi}_\alpha\right)\hat{\omega} + \hat{\phi}_\alpha\hat{a} + g(-Ri_\alpha - \hat{e}_\alpha + v_\alpha)\\ \frac{d\hat{\xi}_\beta}{dt} &= \left(\hat{\chi}_\beta + \frac{1}{\varepsilon}\hat{\phi}_\beta\right)\hat{\omega} + \hat{\phi}_\beta\hat{a} + g\left(-Ri_\beta - \hat{e}_\beta + v_\beta\right)\end{aligned}\right\} \quad (14)$$

and the estimated EMF can be obtained by solving (10):

$$\left.\begin{aligned}\hat{e}_\alpha &= \hat{\xi}_\alpha - gLi_\alpha\\ \hat{e}_\beta &= \hat{\xi}_\beta - gLi_\beta\end{aligned}\right\} \quad (15)$$

From some experiments performed with several PMACMs [14, 15], it has been determined that the induced EMF components obey to the approximation

$$e_\alpha^2 + e_\beta^2 - 4e_0^2 = \omega^2\left(\phi_\alpha^2 + \phi_\beta^2 - 4\phi_0^2\right) \simeq \omega^2 K \quad (16)$$

where K is a coefficient that depends on the motor characteristics. Based on this approximation, the rotor speed can be calculated from (16):

$$\hat{\omega} = \frac{1}{K}\sqrt{\left(\hat{e}_\alpha^2 + \hat{e}_\beta^2 - 4e_0^2\right)} \quad (17)$$

As it can be seen in (17), it is not possible to determine the sign of the estimated speed from this expression. However, it can be demonstrated that the sign of the estimated speed can be calculated by using the expression

$$\left.\begin{aligned}\text{sign}(\hat{\omega}) &\simeq \text{sign}\left(\hat{\phi}_\alpha\frac{d\hat{\phi}_\beta}{dt} - \hat{\phi}_\beta\frac{d\hat{\phi}_\alpha}{dt}\right)\\ &\simeq \text{sign}\left(\hat{\phi}_\alpha\hat{\chi}_\beta - \hat{\phi}_\beta\hat{\chi}_\alpha\right)\end{aligned}\right\} \quad (18)$$

This can easily be proved when ϕ are sinusoidal functions. Then, the estimated speed can be calculated as

$$\hat{\omega} = \frac{1}{K}\text{sign}\left(\hat{\phi}_\alpha\hat{\chi}_\beta - \hat{\phi}_\beta\hat{\chi}_\alpha\right)\sqrt{\left(\hat{e}_\alpha^2 + \hat{e}_\beta^2 - 4e_0^2\right)} \quad (19)$$

From the estimated speed, the estimates of the position derivatives of flux, necessary to implement the torque control law (5), are calculated as follows:

$$\left.\begin{aligned}\hat{\phi}_\alpha &= \frac{\hat{e}_\alpha}{\hat{\omega}}\\ \hat{\phi}_\beta &= \frac{\hat{e}_\beta}{\hat{\omega}}\end{aligned}\right\} \quad (20)$$

As can be seen in (20), this observer cannot be used at very low speed, just like other proposals based on the estimation of the induced EMF. However, a slight change should be included in the algorithm to ensure its proper operation during a speed reversal. If low-speed or standstill operation is needed, the proposed observer should be combined with some open-loop starting procedures or signal-injection techniques, as proposed in the literature [16].

Note that the proposed observer and the sensorless control strategy are based on the model given by (1)–(4), where a constant inductance, a linear friction and inertia were assumed. Parameter uncertainties and nonlinearities can cause the estimation error to converge asymptotically to a small nonzero value. However, it is possible to reduce the asymptotic estimation error by increasing the value of g [17]. In addition, it is well known that mismatches between the motor and the model can affect the drive performance adversely. To overcome this drawback, a PI controller is included in the speed-control loop.

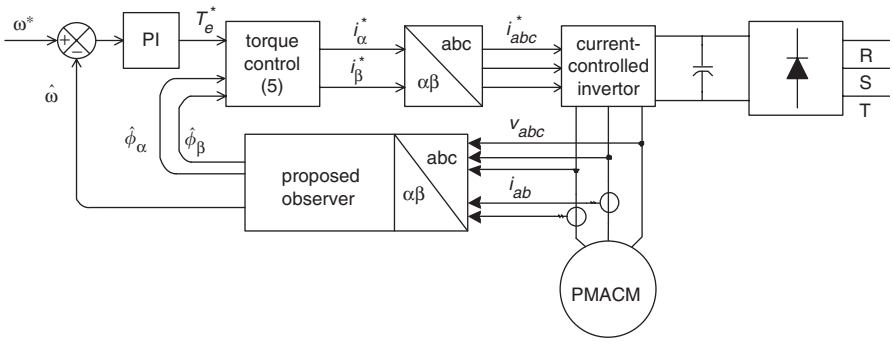

Fig. 1 *Block diagram of the sensorless speed control*

4 Application in a sensorless speed control for different motors

Figure 1 shows a simplified scheme of the proposed sensorless speed control for PMACMs. It has an external speed-control loop fed back by the estimated speed, and an internal torque-control loop. Current references for the invertor current-control loop are generated through (5) by employing the functions estimated by the observer. The implemented algorithm is shown in Appendix 2 (Section 9.2).

In the following paragraphs, some results obtained by numerical simulation of the system shown in Fig. 1 are presented. Three types of motors, with different induced EMF waveforms, were simulated:

(*a*) PMACM with sinusoidal EMF (ideal);

(*b*) PMACM with trapezoidal EMF (ideal); and

(*c*) PMACM which EMF is neither sinusoidal nor trapezoidal (Axial Flux PMACM with experimentally determined waveform).

The same parameters were used for all the motors (see Table 1); the induced EMF waveform being the only change.

The motor is supposed to be driven by a current-controlled PWM voltage-source invertor as shown in Fig. 1. The current references are calculated with the proposed algorithm.

Figures 2–4 show simulation results of the steady-state operation of the three motors under consideration. Figure 2 corresponds to the sinusoidal-EMF PMACM; Fig. 3 to the trapezoidal-EMF PMACM; and Fig. 4 to the axial-flux PMACM. For each motor, the waveform of the position derivative of flux, corresponding to stator phase *a*, is shown in Figs. 2*a*, 3*a* and 4*a*. The actual and estimated components of the position derivative of flux in a stationary reference frame are shown in Figs. 2*b* and *c*, Figs. 3*b* and *c* and Figs. 4*b* and *c*, respectively. It can be seen from these figures that the proposed observer estimates correctly the position derivative of flux for each motor, using only the voltage and current measurements.

In Figs. 2*d*, 3*d* and 4*d*, the simulated electromagnetic torque for the same operating condition is shown. It can be seen that the motor torque has only a high-frequency ripple produced by the switched currents; but the undesired torque harmonics (6th, 12th etc.) [1] have been eliminated.

Figures 5 and 6 show the transient behaviour during start-up, application of unmodelled load torque and speed reversal. Figure 5 shows the actual speed (solid line) and reference speed (broken line) for each motor, when a step speed reference of 250 rev/min is applied to the unloaded

Table 1: Motor and observer parameters

Three-phase permanent-magnet motor	
16 poles, 2000 rev/min	15 KW
$R = 10\,\text{m}\Omega$	$L = 100\,\mu\text{H}$
$J = 0.78\,\text{Kgm}^2$	$B = 0.0015\,\text{Kgm}^2/\text{s}$
$K = 0.5021$	
Observer parameters	
$g = 400$	$\varepsilon = 0.0001$

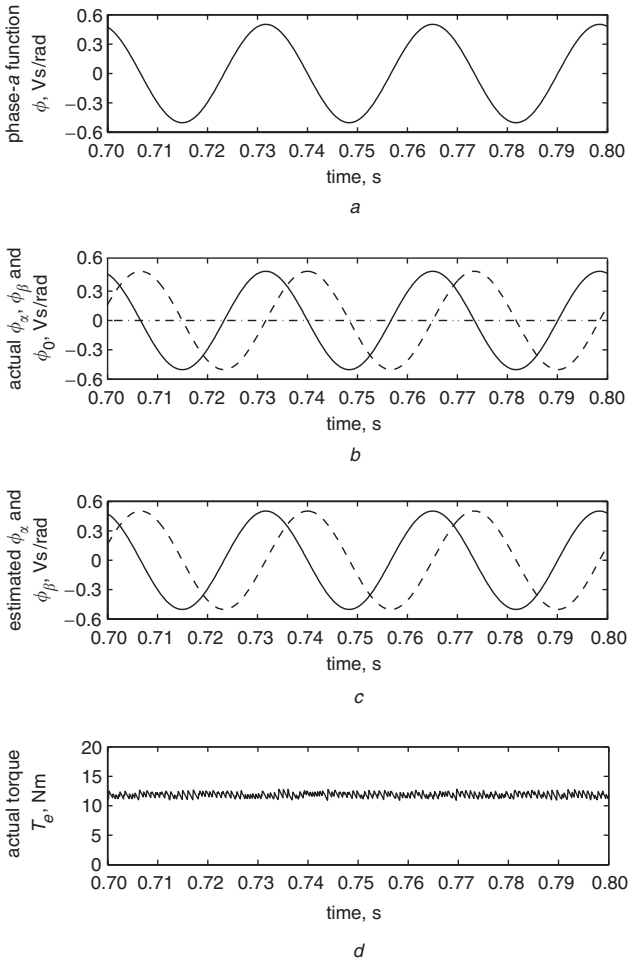

Fig. 2 *Steady-state performance of PMACM with sinusoidal EMF (simulation results)*
a Actual phase-*a* function ϕ
b Actual ϕ_α (solid), ϕ_β (broken) and ϕ_0 (chain dotted)
c Estimated $\hat{\phi}_\alpha$ (solid) and $\hat{\phi}_\beta$ (broken)
d Actual torque T_e

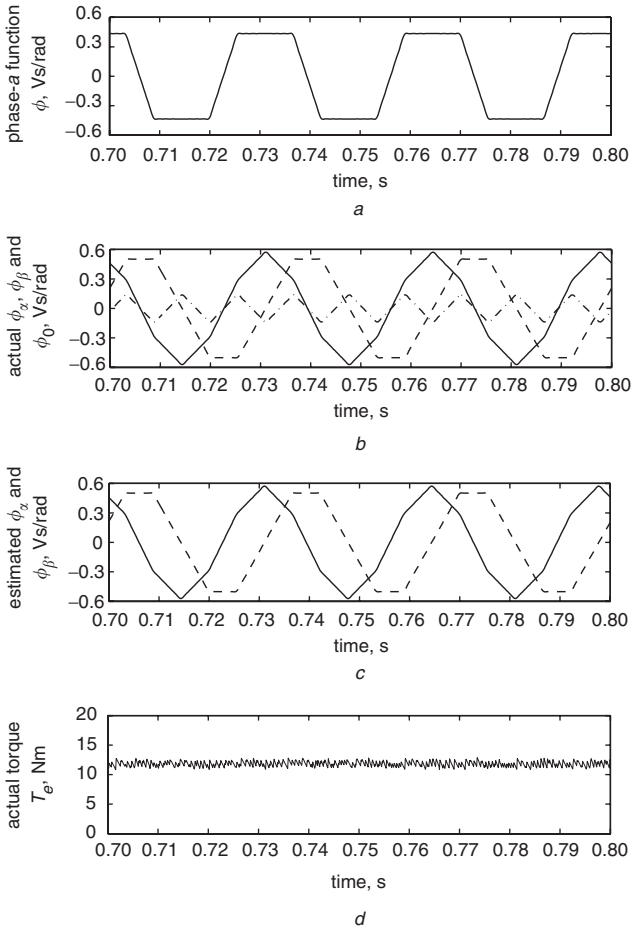

Fig. 3 *Steady-state performance of PMACM with trapezoidal EMF (simulation results)*
a Actual phase-*a* function ϕ
b Actual ϕ_α (solid), ϕ_β (broken) and ϕ_0 (chain dotted)
c Estimated $\hat{\phi}_\alpha$ (solid) and $\hat{\phi}_\beta$ (broken)
d Actual torque T_e

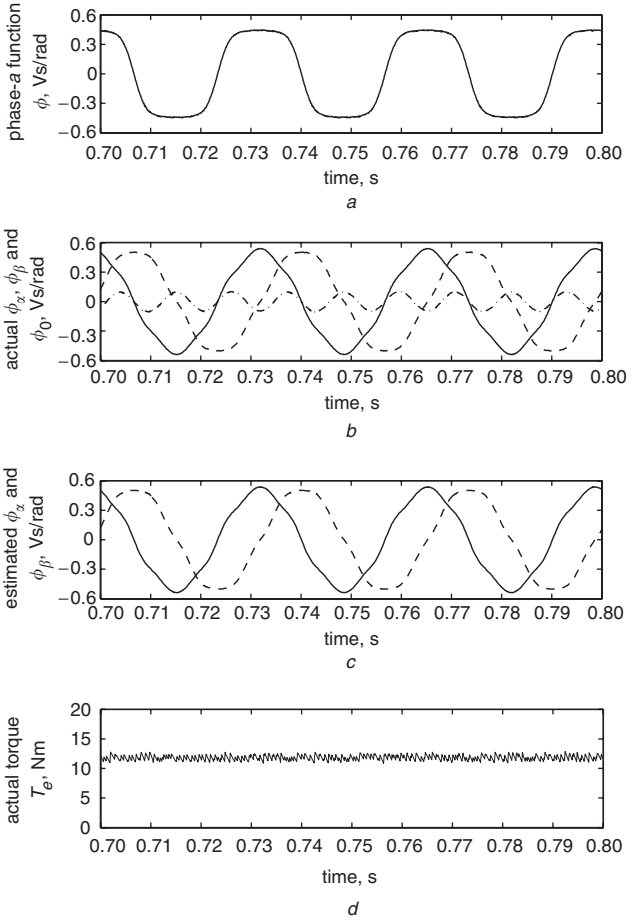

Fig. 4 *Steady-state performance of axial-flux PMACM (simulation results)*
a Actual phase-*a* function ϕ
b Actual ϕ_α (solid), ϕ_β (broken) and ϕ_0 (chain dotted)
c Estimated $\hat{\phi}_\alpha$ (solid) and $\hat{\phi}_\beta$ (broken)
d Actual torque T_e

drive. At 4 s an 8 Nm load torque is applied. All three motors show a good transient response with negligible effect of the nonmodelled load torque.

In Fig. 6 the actual speed (solid line) and reference speed (broken line) during a speed reversal are presented. The three graphs correspond to the three motors under analysis. As stated above, the proposed observer cannot work at zero speed, so hysteresis was added around null speed to allow speed reversal without indetermination. Again, this results show an acceptable closed-loop response even when crossing zero speed.

In summary, simulation results show a good closed-loop response in steady-state and transient operation. The torque ripple is almost negligible when the proposed observer and control strategy are used.

5 Experimental results

To validate the proposed control scheme, a laboratory prototype drive was implemented using an axial-flux PMACM, whose parameters are shown in Table 1. The PMACM motor was fed with a voltage-source invertor with a fast current-control loop. Motor voltages and currents were measured using standard Hall-effect sensors and 12-bit A/D convertors. The acutal speed was also measured, to compare it with the estimated one. The observer and the control strategy were implemented on a PC in 'C' language. Differential equations were discretised using the Euler method with a 200 μs sampling period. The experimental data were captured using a digital scope and plotted with the simulation software for an easier comparison with the simulation results. High-gain observer variables were appropriately scaled to avoid ill-conditioning problems with very small ε values. Note that four differential equations must be solved to implement this observer; therefore it is equivalent to the implementation of previously proposed full-order observers [18] as regards the computational time.

Figure 7 shows the actual (Fig. 7*a*) and estimated (Fig. 7*b*) position derivative of flux when the motor is running at 300 rev/min. As can be seen, the estimated waveform of the position derivative of flux is very similar to the actual waveform. This allows the use of the estimated waveforms to minimise the torque ripple and copper losses. The time derivatives of ϕ_α and ϕ_β, estimated by the high-gain observer, are shown in Fig. 7*c*. The measured current waveforms in the α–β reference frame (i_α, i_β) are shown in Fig. 7*d*.

To test the observer response, initially the motor-drive control loop was closed using the measured variables. A low-speed test is presented in Fig. 8. The unloaded drive is running at 10 rev/min when a sudden change in the reference speed occurs. The estimated and measured speeds

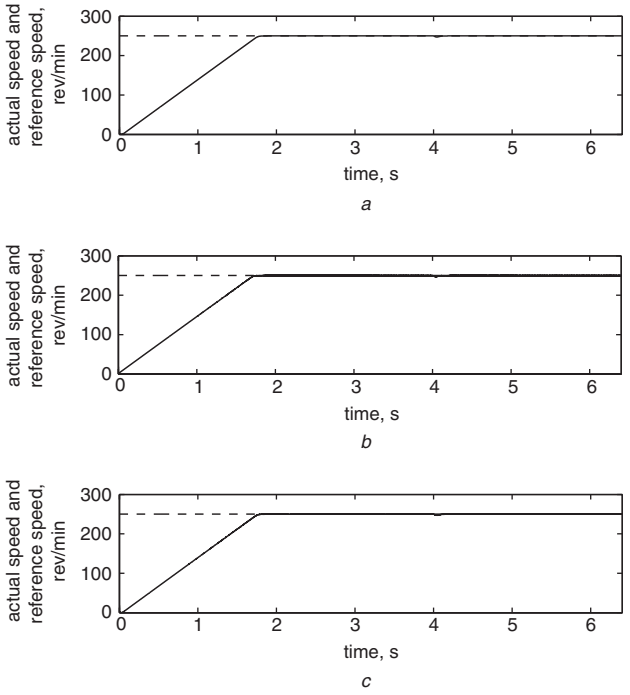

Fig. 5 *Start-up and nonmodelled load-torque test (simulation results)*
Reference speed ω^* (broken) and actual speed ω (solid)
a PMACM with sinusoidal EMF
b PMACM with trapezoidal EMF
c Axial-flux PMACM

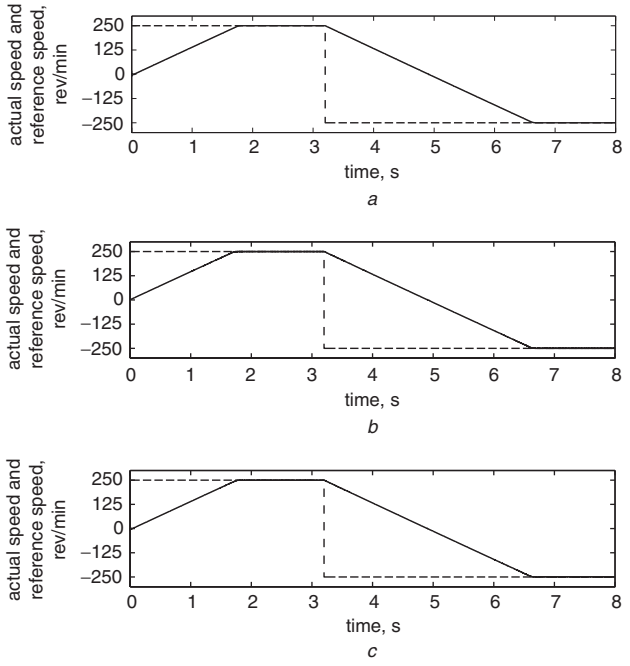

Fig. 6 *Speed-reversal test (simulation results)*
Reference speed ω^* (broken) and actual speed ω (solid)
a PMACM with sinusoidal EMF
b PMACM with trapezoidal EMF
c Axial-flux PMACM

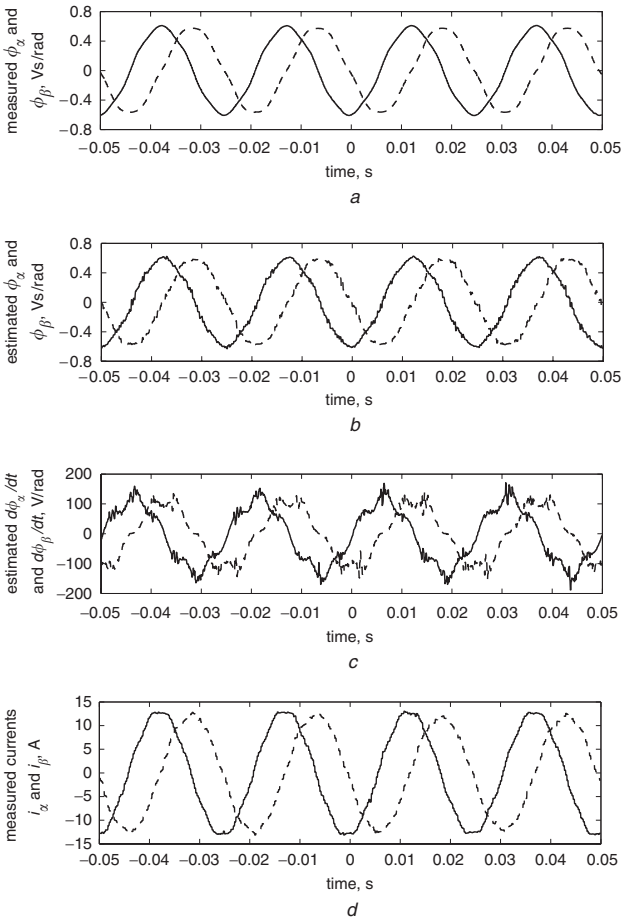

Fig. 7 *Experimental results (variables in a stationary reference frame)*
a Position derivatives of flux ϕ_α (solid) and ϕ_β (broken), measured
b Position derivatives of flux ϕ_α (solid) and ϕ_β (broken), estimated
c Time derivatives of ϕ_α (solid) and ϕ_β (broken), estimated
d Currents waveforms, i_α (solid) and i_β (broken), measured

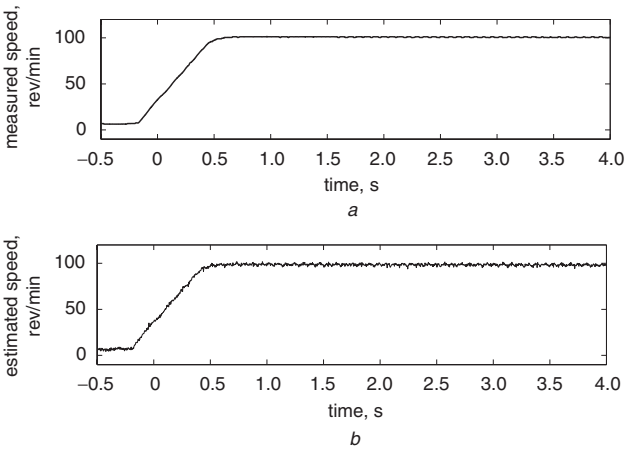

Fig. 8 *Low-speed estimation (experimental results)*
a Measured speed ω
b Estimated speed $\hat{\omega}$

are shown in Fig. 8*a* and *b*, respectively. A speed-reversal test is shown in Fig. 9. It can be seen that the speed sign cannot be determined precisely at low speed, owing to the above mentioned measurement noise.

Figures 10–12 show the closed-loop-drive performance when the estimated variables are used in the control algorithm. A high-speed test is shown in Fig. 10, when the reference speed (broken line) goes from 1000 rev/min to 2000 rev/min. The low-speed test is shown in Fig. 11, when a reference speed profile (100–500–100 rev/min) is applied. In these Figures, a good closed-loop response can be observed, even at low speed and with braking action.

In Fig. 12, an 8 Nm constant load torque is applied at 8 s, in order to test the sensorless-drive response with non-modelled load torque. A small steady-state error appears in

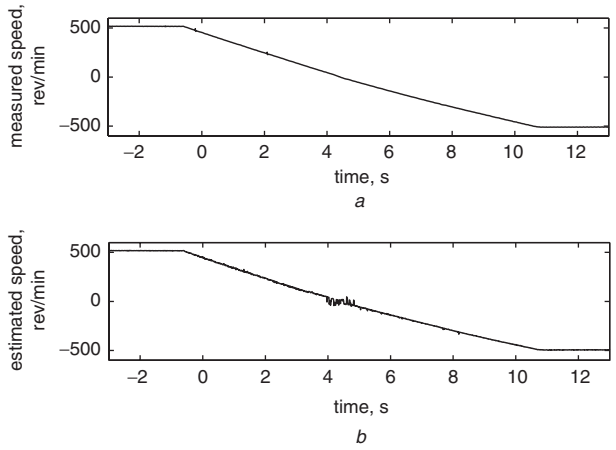

Fig. 9 *Speed-reversal test (experimental results)*
a Measured speed ω
b Estimated speed $\hat{\omega}$

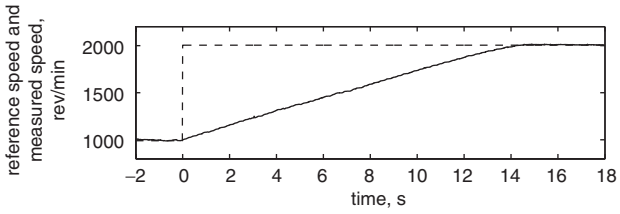

Fig. 10 *Sensorless closed-loop test (high-speed) (experimental results)*
Reference speed (broken line) and actual speed (solid line)

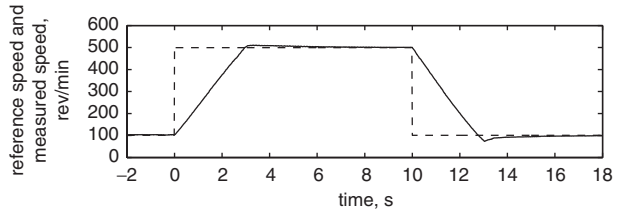

Fig. 11 *Sensorless closed-loop test (low-speed) (experimental results)*
Reference speed (broken line) and actual speed (solid line)

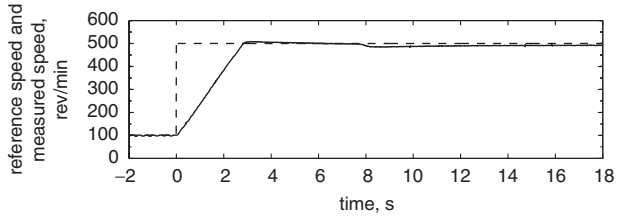

Fig. 12 *Sensorless closed-loop test (low-speed with load torque) (experimental results)*
Reference speed (broken line) and actual speed (solid line)

the motor speed. This small error is produced by the unknown load torque that is not included in the observer model. The observer converges to a small bounded error. If this small error is unacceptable for the drive performance, it can be eliminated by extending the observer as proposed in [19].

6 Conclusions

A sensorless speed-control strategy for permanent-magnet AC motors with nonsinusoidal EMF waveform was presented in this work. The proposed strategy uses a nonlinear reduced-order observer and a high-gain observer to estimate the induced EMF, measuring only the stator currents and voltages. It also allows the reduction of the ripple torque produced by nonsinusoidal EMF waveforms.

Simulation results demonstrate that it is feasible to apply the proposed strategy to PMACMs with almost any EMF waveforms. The proposed strategy was implemented with an axial-flux PMACM whose EMF waveform is neither sinusoidal nor trapezoidal. Experimental results demonstrate a high performance of the observer and a good closed-loop response of the complete sensorless control strategy.

7 Acknowledgments

This work was supported by Universidad Nacional de Río Cuarto (UNRC), Universidad Nacional de La Plata (UNLP), Universidad Nacional del Sur (UNS), FONCyT-ANPCyT and CONICET.

8 References

1 Jahns, T., and Soong, W.: 'Pulsating torque miniminzation techniques for permanent magnet AC motor drives – a review', *IEEE Trans.*, 1996, **IE-43**, (2), pp. 321–330
2 Hanselman, D.: 'Effect of skew, pole count and slot count on brushless motor radial force, cogging torque and back EMF', *IEE Proc. Electr. Power Appl,*. 1997, **144**, (5), pp. 325–330
3 Lam, B., Panda, S., and Xu, J.: 'Periodic torque ripples minimisation in permanent magnet synchronous motor drives using iterative learning control'. Proc. 9th European Conf. Power Electronics and Applications, EPE 2001, Graz, Austria, 2001
4 Holtz, J., and Springob, L.: 'Identification and compensation of torque ripple in high-precision permanent magnet motor drives', *IEEE Trans.*, 1996, **IE-43**, (2), pp. 309–320
5 Cho, K.-Y., Bae, J.-D., Chung, S.-K., and Youn, M.-J.: 'Torque harmonics minimisation in permanent magnet synchronous motor with back EMF estimation', *IEE Proc. Electr. Power Appl.*, 1994, **141**, (6), pp. 323–330
6 Brunsbach, B.-J., Henneberger, G., and Klepsch, T.: 'Compensation to torque ripple'. Proc. Sixth IEE Int. Conf. Electrical Machines and Drives, Oxford, UK, 1993, pp. 588–593
7 Chung, S.-K., Kim, H.-S., Kim, C.-G., and Youn, M.-J.: 'A new instantaneous torque control of PM synchronous motor for high-performance direct-drive applications', *IEEE Trans.*, 1998, **PE-13**, (3), pp. 388–400
8 Leidhold, R., García, G., and Watanabe, E.: 'PMAC Motor control strategy, based on the instantaneous active and reactive power, for ripple-torque and copper-losses minimization'. Proc, IEEE 26th Annual Conf. Industrial Electronics Soc. (IECON'00), Nagoya, Japan, 2000, Vol. 2, pp. 1401–1405
9 Akagi, H., Kanazawa, Y., and Nabae, A.: 'Generalized theory of the instantaneous reactive power in three-phase circuits,'. Proc. Int. Power Electronics Conf. (IPEC'83), Tokyo, Japan, 1983, pp. 1375–1386
10 Johnson, J., Ehsani, M., and Güzelgünler, Y.: 'Review of sensorless mehtods for brushless DC'. Conf. Record 1999 IEEE Industry Applications Conf., 34th IAS Annual Meeting, Phoenix, USA, 1999, Vol. 1, pp. 143–150
11 Krishnan, R.: 'Electric motor drives: modelling, analysis and control' (Prentice Hall, 2001)
12 Solsona, J., Valla, M.I., and Muravchik, C.: 'On speed and rotor position estimation in permanent-magnet AC drives', *IEEE Trans.*, 2000, **IE-47**, (5), pp. 1176–1180
13 Dabroom, A., and Khalil, H.K.: 'Numerical differentiation using high-gain observers'. Proc. 36th IEEE Conf. Decision and Control, San Diego, USA, 1997, Vol. 5, pp. 4790–4795
14 De Angelo, C., Bossio, G., Solsona, J., García, G., and Valla, M.: 'Sensorless speed control of permanent magnet motors with torque ripple minimization' Proc. 28th Annual Conf. IEEE Industrial Electronics Soc., IECON'02, Seville, Spain, 2002, Vol. 1, pp. 680–685
15 De Angelo, C.H.: 'Control para máquinas de CA de imanes permanents con FEM arbitraria, sin sensores mecánicos'. Doctoral thesis, Departamento de Electrotecnia, Facultad de Ingeniería,

Universidad Nacional de La Plata, La Plata, Argentina 2004, (in Spanish). Available: http://sedici.unlp.edu.ar/search/request.php?id_document = ARG-UNLP-TPG-0000000061
16 Linke, M., Kennel, R., and Holtz, J.: 'Sensorless speed and position control of synchronous machines using alternating carrier injection'. Proc. IEEE Int. Electric Machines and Drives Conf. (IEMDC'03), 2003, Vol. 2, pp. 1211–1217
17 Solsona, J.A., and Valla, M.I.: 'Disturbance and nonlinear Luenberger observers for estimating mechanical variables in permanent magnet synchronous motors under mechanical parameters uncertainties', *IEEE Trans.*, 2003, **IE-50**, (4), pp. 717–725
18 Zhu, G., Kaddouri, A., Dessaint, L.-A., and Akhrif, O.: 'A nonlinear state observer for the sensorless control of a permanent-magnet AC machine', *IEEE Trans.*, 2001, **IE-48**, (6), pp. 1098–1108
19 Solsona, J., Valla, M.I., and Muravchik, C.: 'Nonlinear control of a permanent magnet synchronous motor with disturbance torque estimation', *IEEE Trans.*, 2000, **EC-15**, (2), pp. 163–168

9 Appendixes

9.1 Reduced-order high-gain observer

The reduced-order high-gain observer used to obtain the time derivatives of $\hat{\phi}$ can be constructed as follows [13]. Setting

$$\left.\begin{aligned} x_1 &= \hat{\phi} \\ x_2 &= \frac{dx_1}{dt} = \frac{d\hat{\phi}}{dt} \end{aligned}\right\} \tag{21}$$

where $\hat{\phi}$ is known (sub-indexes corresponding to α–β components have been suppressed for clarity), and defining

$$\left.\begin{aligned} \hat{x}_1 &= \tilde{\phi} \\ \hat{x}_2 &= \frac{d\hat{x}_1}{dt} = \frac{d\tilde{\phi}}{dt} \end{aligned}\right\} \tag{22}$$

it is desired to estimate x_2 without estimating x_1. Then the following observer is proposed:

$$\frac{d\hat{x}_2}{dt} = \frac{1}{\varepsilon}\left(\frac{dx_1}{dt} - \frac{d\hat{x}_1}{dt}\right) \tag{23}$$

where ε is a small positive parameter. To avoid the calculation of dx_1/dt, a variable change is proposed:

$$\hat{X} = \hat{x}_2 - \frac{1}{\varepsilon}x_1 \tag{24}$$

Taking the time derivative of (24), and replacing from (23), the reduced-order observer results in

$$\frac{d\hat{\chi}}{dt} = -\frac{1}{\varepsilon}\left(\hat{X} + \frac{1}{\varepsilon}x_1\right) \tag{25}$$

and

$$\hat{x}_2 = \hat{\chi} + \frac{1}{\varepsilon}x_1 \tag{26}$$

Returning to the original variables, the reduced-order high-gain observer results in

$$\frac{d\hat{\chi}}{dt} = -\frac{1}{\varepsilon}\left(\hat{\chi} + \frac{1}{\varepsilon}\hat{\phi}\right) \tag{27}$$

and

$$\frac{d\tilde{\phi}}{dt} = \hat{\chi} + \frac{1}{\varepsilon}\hat{\phi} \tag{28}$$

9.2 Proposed observer algorithm

(*a*) Initial conditions: $\hat{\omega}(0)$, $\hat{\phi}_\alpha(0)$, $\hat{\phi}_\beta(0)$, $\hat{\chi}_\alpha(0)$, $\hat{\chi}_\beta(0)$

(*b*) Inputs: $i_\alpha, i_\beta, \upsilon_\alpha, \upsilon_\beta, \upsilon_0$

(*c*) Algorithm:

$$\hat{a} = \frac{d\hat{\omega}}{dt} = \frac{1}{J}\left(\hat{\phi}_\alpha i_\alpha + \hat{\phi}_\beta i_\beta\right) - \frac{B}{J}\hat{\omega} \tag{29}$$

$$\left.\begin{aligned} \frac{d\hat{\xi}_\alpha}{dt} &= \left(\hat{\chi}_\alpha + \frac{1}{\varepsilon}\hat{\phi}_\alpha\right)\hat{\omega} + \hat{\phi}_\alpha\hat{a} + g(-Ri_\alpha - \hat{e}_\alpha + v_\alpha) \\ \frac{d\hat{\xi}_\beta}{dt} &= \left(\hat{\chi}_\beta + \frac{1}{\varepsilon}\hat{\phi}_\beta\right)\hat{\omega} + \hat{\phi}_\beta\hat{a} + g(-Ri_\beta - \hat{e}_\beta + v_\beta) \end{aligned}\right\} \tag{30}$$

$$\left.\begin{aligned} \frac{d\hat{\chi}_\alpha}{dt} &= -\frac{1}{\varepsilon}\left(\hat{\chi}_\alpha + \frac{1}{\varepsilon}\hat{\phi}_\alpha\right) \\ \frac{d\hat{\chi}_\beta}{dt} &= -\frac{1}{\varepsilon}\left(\hat{\chi}_\beta + \frac{1}{\varepsilon}\hat{\phi}_\beta\right) \end{aligned}\right\} \tag{31}$$

$$\left.\begin{aligned} \hat{e}_\alpha &= \hat{\xi}_\alpha - gLi_\alpha \\ \hat{e}_\beta &= \hat{\xi}_\beta - gLi_\beta \end{aligned}\right\} \tag{32}$$

$$\hat{\omega} = \frac{1}{K}sign\left(\hat{\phi}_\alpha\hat{\chi}_\beta - \hat{\phi}_\beta\hat{\chi}_\alpha\right)\sqrt{\left(\hat{e}_\alpha^2 + \hat{e}_\beta^2 - 4e_0^2\right)} \tag{33}$$

$$\left.\begin{aligned} \hat{\phi}_\alpha &= \frac{\hat{e}_\alpha}{\hat{\omega}} \\ \hat{\phi}_\beta &= \frac{\hat{e}_\beta}{\hat{\omega}} \end{aligned}\right\} \tag{34}$$